Computers in Biology and Medicine 116 (2020) 103529

Contents lists available at ScienceDirect

Computers in Biology and Medicine

journal homepage: http://www.elsevier.com/locate/compbiomed

Original Article

Relationship between lower lumbar spine shape and patient bone metabolic activity as characterised by ^{18}F NaF bio-markers

S. Yeung [a], A. Toor [b], G. Deib [c], J. Zhang [a], T. Besier [a,d], J. Fernandez [a,d,*]

[a] Auckland Bioengineering Institute, University of Auckland, Auckland, New Zealand
[b] Auckland District Health Board, Auckland, New Zealand
[c] Centre for Advanced MRI, University of Auckland, Auckland, New Zealand
[d] Department of Engineering Science, University of Auckland, Auckland, New Zealand

ARTICLE INFO

Keywords:
NaF PET-CT
Lower lumbar
Principal component analysis
Lower lumbar pathology
Bone metabolic activity

ABSTRACT

Chronic lower lumbar pain has been associated with elevated bone metabolic activity in the spine. Diagnosis of bone metabolic activity is currently through integrating Positron Emission Tomography (PET) with Sodium Fluoride (^{18}F–NaF) biomarkers. It has been reported that numerous observable pathologies including lumbar fusion, disc abnormalities and scoliosis have often been associated with increased ^{18}F–NaF uptake. The aim of this study was to identify what features of lower lumbar shape most strongly correlate with ^{18}F–NaF uptake. Following a principal component analysis of 23 patients who presented with lumbar pain and underwent ^{18}F–NaF PET-CT, it was revealed that three modes interpreted as (i) sacral tilt, (ii) vertebral disc spacing and (iii) spine size were the three characteristics that described 88.7% of spine shape in our study population. ^{18}F–NaF was described by two modes including ^{18}F–NaF intensity and spatial variation (anterior-inferior to posterior-superior). ^{18}F–NaF was most sensitive to sacral tilt followed by vertebral disc spacing. A predictive model derived from that spine population was able to predict ^{18}F–NaF 'hot-spot' locations with 85 ± 5% accuracy and with 71 ± 3% accuracy for the ^{18}F–NaF magnitude. These results suggest that patients reporting with lower lumbar pain and who present with increased sacral tilt profiles and/or reduced disc spacing are good candidates for further ^{18}F–NaF PET-CT imaging, evidenced by the high association between those shape profiles and ^{18}F–NaF uptake.

1. Introduction

Chronic patient bone pain has been associated with elevated metabolic activity as illustrated in the patellofemoral joint [1] and the spine [2]. A commonly used assessment of bone metabolic activity in the musculoskeletal system is integration of Positron Emission Tomography (PET) with Sodium Fluoride (^{18}F–NaF) biomarkers [3]. Computed Tomography (CT) is used to reference the low spatial-resolution PET imaging to high spatial resolution bone anatomy. Lower back pain [4,5] is typically experienced in the lower vertebral column, sacral and coccygeal regions [6], and surrounding tissues [7–9]. The ^{18}F–NaF biomarker has a high affinity for changes in metabolic bone activity that has been associated with pain receptors in bone [1], osteoarthritis [10,11] and site specific bone remodelling following drug treatment [12]. It does not identify soft tissue, hence, we are not concerned with soft tissue origins of metabolic activity in this study.

Sodium fluoride (^{18}F–NaF) is a biomarker injected into patients before PET scans as an imaging agent that identifies osteogenic activity [13]. The use of ^{18}F–NaF exposes the patient to ionising radiation and is commonly used in clinics to identify and track bone metastases [14,15] and evaluating lesions following spontaneous osteonecrosis (bone tissue death) [16]. A review of the use of ^{18}F–NaF highlighted excellent diagnostic performance for the detection of bone tumours, but the higher ionising dosage and cost were raised as issues over other modalities such as planar bone scintigraphy [17].

There have been numerous non-oncologic uses of ^{18}F–NaF PET-CT reported in the musculoskeletal system [18]. Specifically, given ^{18}F–NaF PET-CT has been associated with spinal geometry variations including joint and disc abnormalities [2], lumbar fusion and scoliosis [19] and spinal stenosis [20], this suggests that specific spinal shape profiles may be associated with ^{18}F–NaF uptake. A common tool for assessing shape in engineering and biology is principal component

* Corresponding author. Auckland Bioengineering Institute University of Auckland, New Zealand.
E-mail address: j.fernandez@auckland.ac.nz (J. Fernandez).

https://doi.org/10.1016/j.compbiomed.2019.103529
Received 20 July 2019; Received in revised form 31 October 2019; Accepted 31 October 2019
Available online 3 November 2019
0010-4825/© 2019 Elsevier Ltd. All rights reserved.

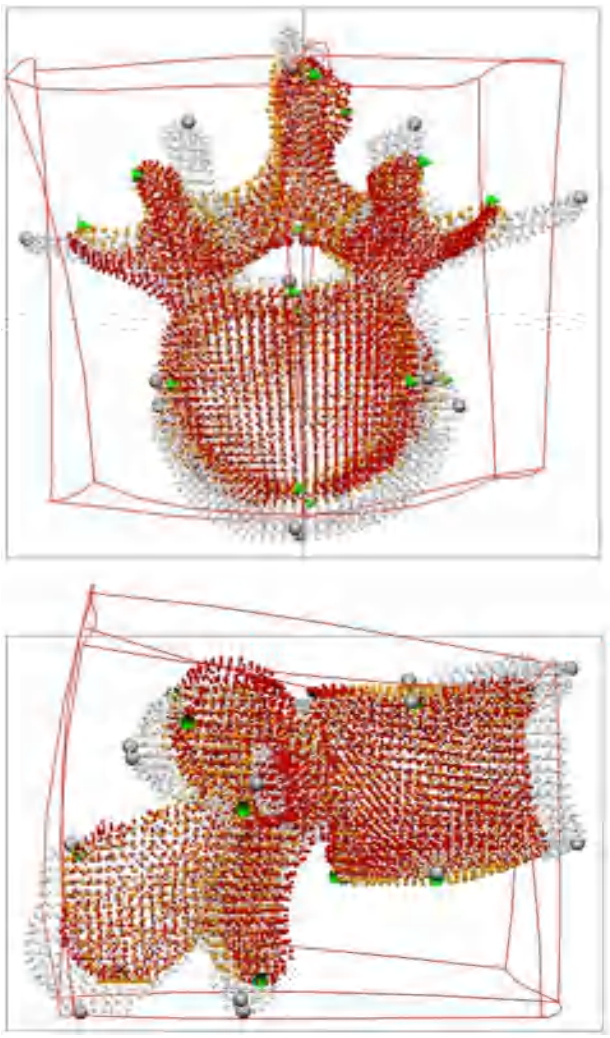

Fig. 1. Initial host-mesh (grey box) is deformed to the red box to minimise the distance between landmark points (grey spheres) and target points (green cones). As a result, the generic vertebrae (grey) is deformed to the red vertebrae. The actual patient vertebra is shown in gold.

analysis and partial least squares regression to identify key variational features in populations and correlate these to more measurable features [21–26]. Previous demonstrations in spine mechanics include 3D shape prediction of postoperative trunks for non-invasive scoliosis surgery planning [27], multivariate biomechanical measurements of the spine during a rowing exercise [28], and bone mass variation in lumbar vertebrae and femoral regions [29].

This study aims to investigate a patient population who presented with lower lumbar pain and had ^{18}F–NaF PET-CT. We firstly aim to identify the bone shape characteristics that describe the lower lumbar population using principal component analysis. Secondly, we aim to describe the variation of ^{18}F–NaF uptake in the spine. Thirdly, a partial least squares regression statistical model is presented, correlating lower lumbar shape profiles with ^{18}F–NaF uptake to investigate ^{18}F–NaF sensitivity to spinal shape. The statistical model is then evaluated by predicting ^{18}F–NaF uptake in patients from lower lumbar shape.

2. Methods

Twenty-three patients who presented with lower lumbar pain and had undergone ^{18}F–NaF PET-CT at a local private hospital were used in this study. Ethical approval was obtained prior to the data collection by the local ethics advisory board. The population consisted of 12 females (mean age 43.3 ± 16.5 years; mean Body Mass Index (BMI) $26.9 \pm 7.13\,kg/m^2$) and 11 males (mean age 46.2 ± 19.4 years; mean BMI $27.0 \pm 4.89\,kg/m^2$). The combined population showed an average age of 44.7 ± 17.6 years and BMI of $27.0 \pm 6.02\,kg/m^2$, respectively.

CT data sets of the lower spine were used to create an anatomical 3D surface mesh representation of the L3, L4, L5, sacrum and coccygeal bones for each patient. The CT images were segmented and divided into separate bone objects using the segmentation software Stradwin[1] and HyperMesh[2] (geometric meshing software). The models were orientated according to an anatomical sacral coordinate system. The first axis was defined between the superior vertices of the sacrum (this is the bending-flexion axis). A second axis was then defined from the midpoint of the superior vertices to the most inferior vertex of the sacrum (this is the rotation axis). The third axis was the cross-product (this is the side bending axis). This sacral coordinate system could be defined easily in CT by detecting the extreme bony edges. Hence, all shape modes derived in this study are with respect to this coordinate system. The models were then created in CMISS[3] (a custom mesh visualisation software) using a 'host mesh' free-form deformation fitting technique [30], where a generic spinal vertebrae was morphed into a target vertebra using a least squares approximation. In order to solve this, we used an iterative closest point algorithm to solve the least squares minimisation where the objective function that is minimised is:

$$F(u_n) = \sum_{d=1}^{N} W_d ||u_d - z_d|\,|^2, \tag{1}$$

where z_d are the geometric coordinates of the target points of the new vertebra, w_d is a weighting for each control point, and u_d are the landmark points on the original generic vertebrae interpolated inside the host-mesh. Algorithm details and use of this method are detailed in Fernandez et al. [30]. Fig. 1 demonstrates how each vertebra was embedded in a host-mesh (grey) and deformed (red box) so as to minimise the difference between anatomical targets (shown as grey spheres). The initial vertebra (in grey) is deformed to best-match the red vertebrae. The was repeated for all 23 data sets in order to produce models with consistent topology that is required in order to perform principal component analysis.

Fig. 2 outlines the modelling pipeline used in this study. In the ^{18}F–NaF population, an intensity uptake model was created to represent each subject's^{18}F–NaF concentration by mapping intensity values from CT scans onto each corresponding anatomical lower spine geometry. The ^{18}F–NaF intensity was normalised across patients by setting the maximum of each patient to the intensity of the pooled ^{18}F–NaF values within their bladder. The ^{18}F–NaF PET images were standard 200×200 pixel grey-scale DICOM images, which assisted with consistent filtering and image processing across the entire population. ^{18}F–NaF was extracted from axial slice PET imaging and mapped to each subject's spine model by assigning ^{18}F–NaF intensity values to vertebral nodes using a closest-fit algorithm [31]. After mapping to each subject a Gaussian smoothing filter was applied to reduce noise.

Principal component analysis (PCA) was performed on the anatomical modes and ^{18}F–NaF uptake distribution separately. PCA is a statistical analysis technique using matrix decomposition to find orthogonal vectors (principal components), which represent characteristic variations (modes) within a data set [32]. PCA was adapted from the open-source machine learning library (Scikit learn, http://scikit-learn.org/stable/) and applied to the 23 patient data sets. PCA modes were identified and associated with anatomical descriptions in descending order of importance and reconstructed for visualisation in the custom Physiome visualisation tool CMGUI (http://physiomeproject.org/softw

[1] http://mi.eng.cam.ac.uk/~rwp/stradwin/.
[2] www.altairhyperworks.com.
[3] www.cmiss.org.

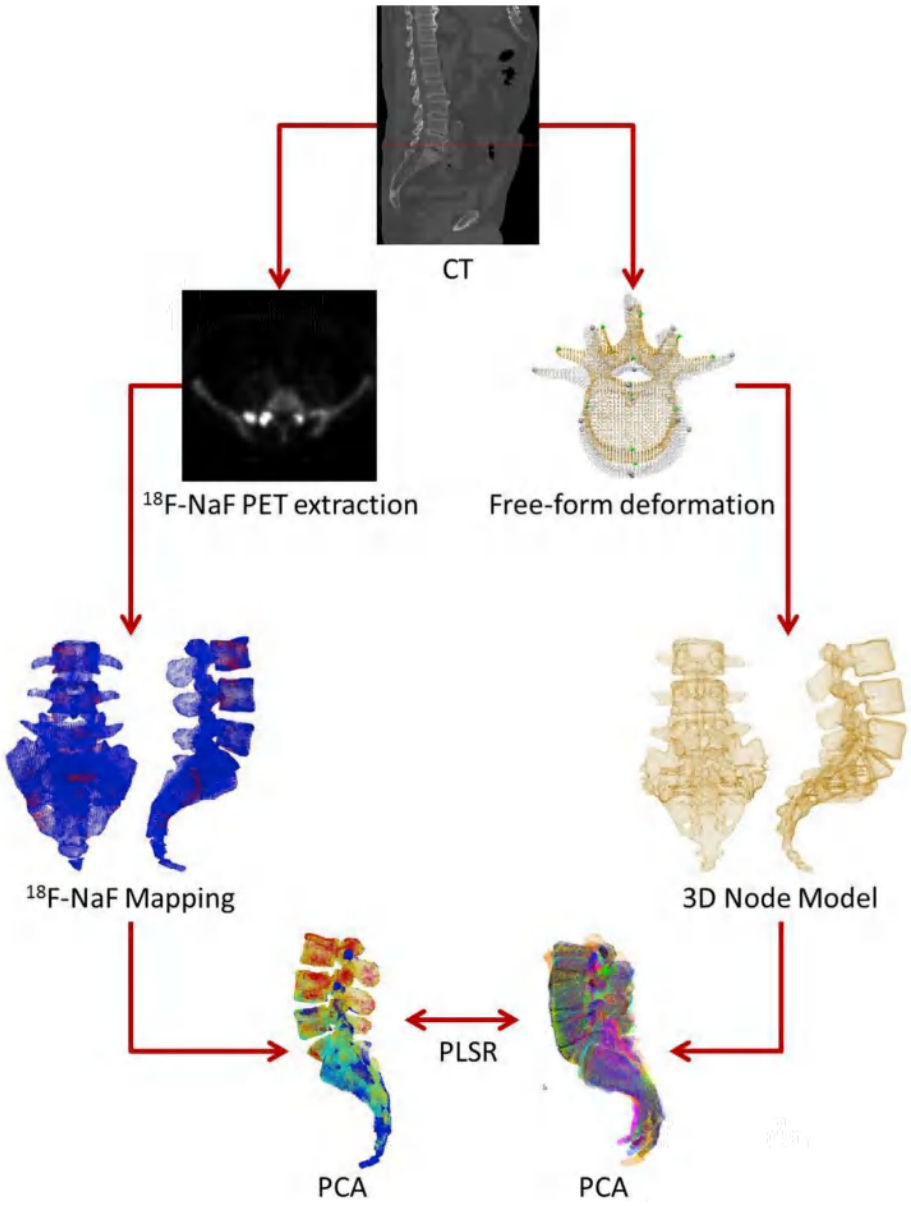

Fig. 2. Framework diagram shows: (left) extracting patient geometry information from sagittal CT scans, then using free-form deformation to create 3D node models used for PCA of shape; (right) extraction of ^{18}F–NaF from axial slice PET-CT, mapping the intensity values onto each patient's respective 3D geometry for PCA of ^{18}F–NaF uptake. PLSR for correlations between ^{18}F–NaF uptake and lower lumbar shape.

are/opencmiss/cmgui).

Partial Least Squares Regression (PLSR) [33] was used to establish a correlation between anatomical spinal shape and ^{18}F–NaF uptake. PLSR was used to model the relationships between PCA modes of shape and PCA modes of ^{18}F–NaF uptake. The two fundamental equations in PLSR are the predictor matrix (X) and the response matrix (Y) given by

$$X_{NM} = T_{NL}\ P^{T}_{ML} + E_{NM}, \tag{2}$$

and

$$Y_{NP} = U_{NL}\ Q^{T}_{PL} + F_{NP}, \tag{3}$$

where N is the number of data sets (23 in this study), M is the number of predictor variables (shape PCA modes), P is the number of response variables (^{18}F–NaF PCA modes), and L is the number of principal components. $\boldsymbol{T}$ and $\boldsymbol{U}$ are the projection matrices (also known as scores), and P and Q are transposed orthogonal loading matrices (where the rows are created from eigenvectors or principal components), and E and F are the error or residual terms. The score vectors are related using a linear function

$$U = f(T) + H, \tag{4}$$

where $\boldsymbol{H}$ is a vector of residuals. The PLSR model was evaluated using a 'leave-one-out' method by excluding the current patient from the training model and using it for testing, then swapping to the next patient and repeating the process. To identify sensitivity between spinal shape and ^{18}F–NaF uptake, modes of spine shape variation were perturbed by ± 2 standard deviations to observe the effect on ^{18}F–NaF uptake intensity and spatial change.

3. Results

PCA shape modes revealed the main characteristic shape variations found within the lower lumbar spine, and their significance can by interpreted as (i) sacral tilt (61.7%), (ii) vertebral disc spacing (15.7%),

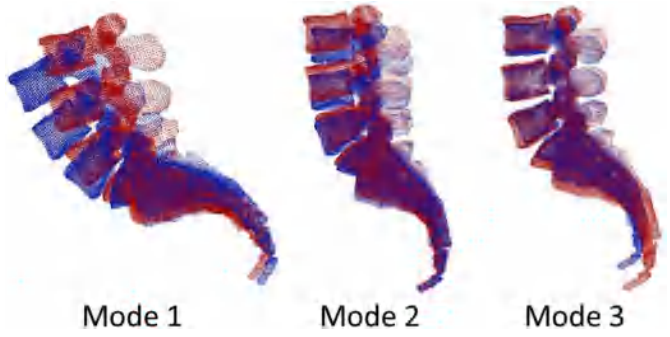

Fig. 3. Principal component modes 1 to 3 showing mode of variation from the mean (blue) to the '+2' standard deviation (red). Mode 1 represents sacral tilt; mode 2 is vertebral spacing; mode 3 represented scaling of size.

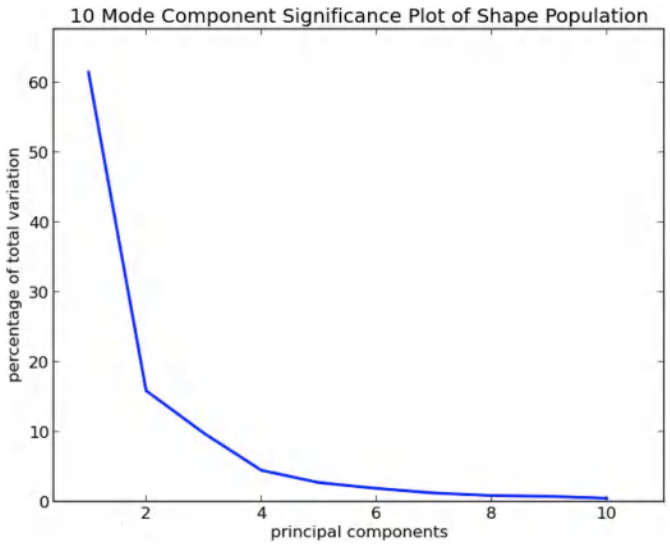

Fig. 4. Line graph of the percentage of total variation for each principal component modes 1 to 10 for whole shape population (23 patients).

and (iii) scaling of size (11.3%) as seen in Fig. 3. Only the top three modes of variation exhibited anatomical definable characteristics of shape accounting for 88.7% of the variation in lower lumbar spine shape (Fig. 4). The PCA modes of variation for ^{18}F–NaF uptake (Fig. 5) were observed as (i) ^{18}F–NaF overall intensity (64.3%), and (ii) an anterior-inferior to posterior-superior intensity shift (7.5%). Only these two variations were distinguishable in terms of anatomy.

PLSR predicted ^{18}F–NaF uptake intensity with a 71 ± 3% accuracy (averaged across all elements), and 85 ± 5% for the pattern of ^{18}F–NaF uptake. Qualitative evaluation revealed that predicted ^{18}F–NaF spatial variation and pattern was modelled better than intensity values using PLSR, with magnitudes of peak ^{18}F–NaF uptake often over or under predicted. Sensitivity analysis using the PLSR model showed that a 10% increase of sacral tilt exhibited a 6.5% increase in ^{18}F–NaF intensity, a 10% increase in vertebral disc spacing resulted in a 5.1% increase in ^{18}F–NaF intensity, and a 10% increase in spinal size resulted in a 1.7% increase in ^{18}F–NaF intensity.

A further sensitivity analysis on the spatial variation of ^{18}F–NaF uptake in response to spinal shape change was investigated. Fig. 6 highlights the effect of perturbing the PLSR model by ± 2 S. D along each mode to explore the effect of shape on ^{18}F–NaF intensity variation. The first vertical line represents the first mode, and then follows a clockwise direction of increasing modes. The results show that the predicted ^{18}F–NaF for ±2 S. D of the first shape mode (which was interpreted as sacral tilt) produced the strongest ^{18}F–NaF intensity variation

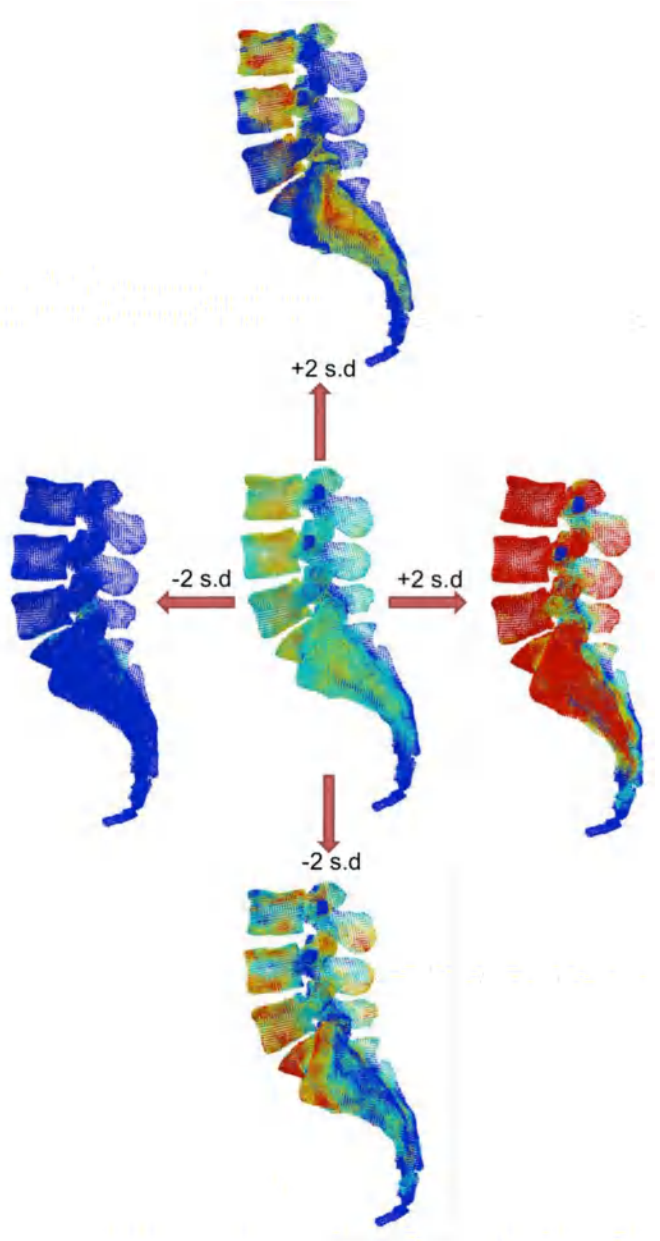

Fig. 5. PCA of ^{18}F–NaF distribution around the centre mean. Left to Right is ± 2sd for mode 1 and Top to Bottom is ± 2sd for mode 2. Red represents high ^{18}F–NaF intensity distribution and blue being no/little ^{18}F–NaF intensity.

throughout the lower lumbar spine. The second most significant mode (interpreted as vertebral disc spacing) produced a predicted ^{18}F–NaF response pattern that moved posteriorly and anteriorly. Perturbation of the third mode of shape (interpreted as spine size) exhibited a subtle superior and inferior shift of ^{18}F–NaF along the length of the spine. For completeness, the 4th shape mode was modelled and showed a subtle medial-lateral spine variation producing subtle variations of ^{18}F–NaF intensity primarily in the sacrum.

The PLSR model was evaluated for ^{18}F–NaF response given lower lumbar spinal shape as a clinical predictor. Fig. 7, shows three examples of predicted ^{18}F–NaF uptake and their respective 'real' ^{18}F–NaF uptake from PET-CT. Fig. 7a, shows predicted ^{18}F–NaF intensity concentrated around the L5 to sacrum (anterior sacral promontory) area. There is also ^{18}F–NaF uptake on the anterior-inferior L5 body, superior L4 spinous process, and the inferior L3 spinous process, which the prediction model captures well but with over-prediction of ^{18}F–NaF magnitude. Fig. 7b

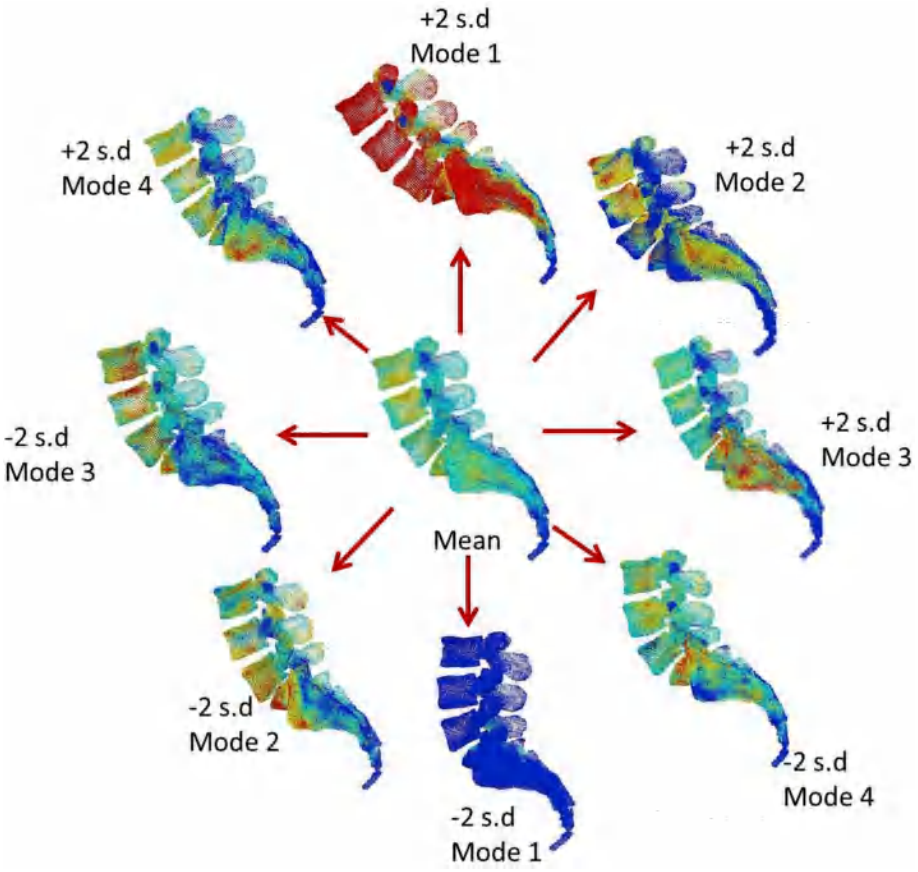

Fig. 6. Effects of PLSR predicted ^{18}F–NaF uptake from perturbing PCA shape modes 1 (sacral tilt), 2 (vertebral disc spacing), 3 (spinal size), and 4 (unidentifiable anatomical shape characteristic). Red represents high ^{18}F–NaF intensity distribution and blue being no/little ^{18}F–NaF intensity.

exhibits a patient with ^{18}F–NaF uptake concentrated primarily on the posterior sacral promontory and posterior L5 centrum region, and the PLSR prediction shows a strongly correlated pattern. The patient in Fig. 7c showed ^{18}F–NaF uptake in the L5 vertebral region and the PLSR model predicted this site as well but with lower intensity. However, the PLSR model also predicted ^{18}F–NaF uptake on the L3 inferior articular process, which was not observed in the patient. Quantitatively, we found PLSR predicted ^{18}F–NaF uptake with an average accuracy of 71 ± 3% of the actual ^{18}F–NaF uptake intensity, and 85 ± 5% of the ^{18}F–NaF uptake pattern, across 23 spines using a 'leave-one-out' analysis across all spines.

4. Discussion

The aims of this study were to identify the features of shape that describe the lower lumbar population, describe the variation of ^{18}F–NaF uptake across the spine, develop a partial least squares regression that relates lower lumbar shape to ^{18}F–NaF uptake, use that model to identify what features of shape are most correlated to ^{18}F–NaF uptake, and to predict ^{18}F–NaF uptake from knowing lower lumbar shape. This may have useful clinical implications by assisting to identify patients at risk of bone degeneration using simple planar imaging of patients who present with lower back pain. Following a PCA of 23 patients it was revealed that modes interpreted as sacral tilt, vertebral disc spacing and spine size were the three characteristics that described spine shape accounting for 88.7% of the variation in our study population. ^{18}F–NaF was described by two modes including ^{18}F–NaF intensity and spatial variation (anterior-inferior to posterior-superior). ^{18}F–NaF was most sensitive to sacral tilt followed by vertebral disc spacing. A predictive model derived from that spine population was able to predict the pattern of ^{18}F–NaF 'hot-spots' with 85 ± 5% accuracy but was less able to predict the intensity of ^{18}F–NaF uptake (71 ± 3%).

This study used PCA to characterise shape variations in the lower lumbar and PLSR to correlate those lower lumbar shape variations with ^{18}F–NaF uptake (a surrogate for metabolic bone activity). The three main principal components (shape characteristics) found in this study for the lower lumbar were interpreted as sacral tilt (also termed lumbar lordosis), vertebral disc spacing, and spinal size, explaining 88.7% of spinal shape variation. No PCA models confined to the lower lumbar spine have been reported in the literature to date, however, a previous PCA model of spine reported capturing 90% of shape variation using four modes for the whole spine in scoliotic patients [34]. In that study they reconstructed the geometries and correlated the modes to patient growth (size), double thoraco-lumbar curve, thoracic curve, and lumbar lordosis, in that order. A difference between the order of modes in that study and the present model is that they investigated the complete spine in a pathologic group (scoliosis). Hence, size is likely the largest mode followed by scoliotic variations seen in both the thoracic and lumbar regions. Their shape modes were also confounded between the thorax and lower lumbar, hence, the double thoraco-lumbar characterisation. Compared to our study, we analysed the lower lumbar in a mature aged size-limited population, hence, sacral tilt was the largest variation identified (lumbar lordosis), which was also a shape mode reported by Boisvert, Pennec, Labelle, Cheriet and Ayache [34]. Both studies found that 88–90% of shape variations could be captured by 3–4 modes.

PCA has previously been adopted to visualise and classify PET imaging in pathologic data. Thireou, Strauss, Dimitrakopoulou-Strauss, Kontaxakis, Pavlopoulos and Santos [35] reported the PCA modes were correlated with anatomical accumulation sites of radioactive biomarkers. In the current study we used a similar technique to characterise the spatial migration and affinity to bone of ^{18}F–NaF. The major mode of ^{18}F–NaF variation identified across our study population was uptake

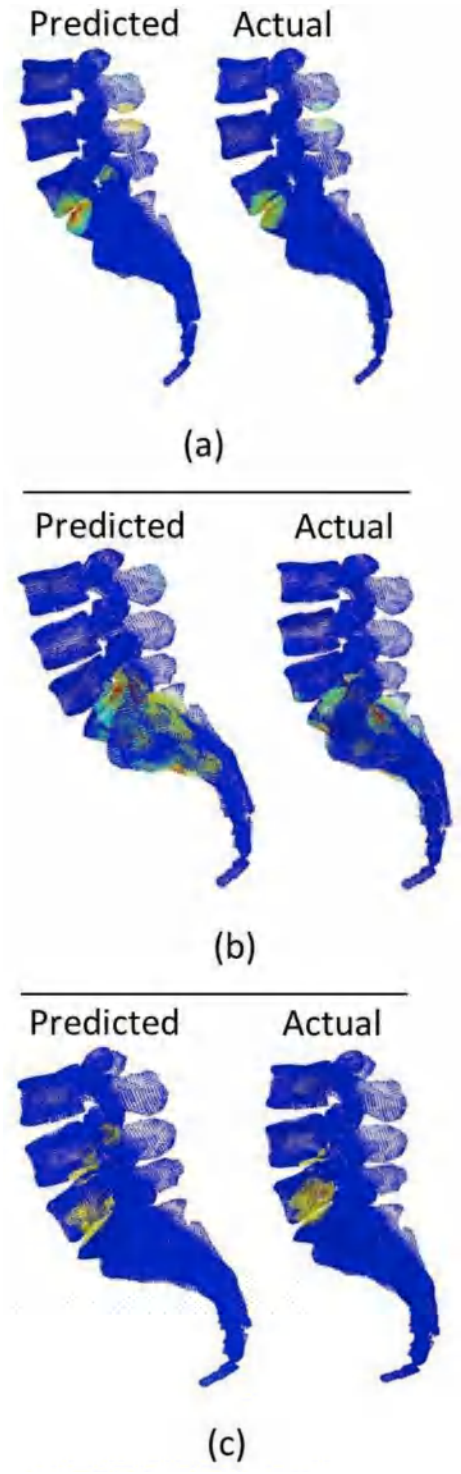

Fig. 7. PLSR predicted ^{18}F–NaF distribution versus actual ^{18}F–NaF uptake pattern for patients A, B and C. Red represents high ^{18}F–NaF intensity distribution and blue being no/little ^{18}F–NaF intensity.

intensity, characterised by the presence (all red) or the lack (all blue) of ^{18}F–NaF (Fig. 6). This was consistent with the first mode reported by Thireou, Strauss, Dimitrakopoulou-Strauss, Kontaxakis, Pavlopoulos and Santos [35] who reported the primary variation as all structures present with a biomarker. The second mode of ^{18}F–NaF variation identified across our study population was a spatial translation from the superior-posterior lumbar region to the inferior-anterior sacral region. This mode aligns with the two main postures and loading patterns observed in the lumbar spine. Patient anterior sacral tilt (lordosis) corresponds with loading along the posterior sacrum and anterior columns of L3 and L4, where ^{18}F–NaF was observed, and posterior sacral tilt corresponds with loading along the anterior sacrum and L5, where ^{18}F–NaF is observed.

PLSR revealed the relationship between spinal shape variation and location of ^{18}F–NaF uptake. The ^{18}F–NaF intensity was most sensitive to sacral tilt, which in extreme anterior pelvic tilt is classified as hyperlordosis causing extreme compression in the sacral region, a precursor to bone degeneration and lower back pain [36]. Vertebral disc spacing was the second most influential factor and corresponded well to degeneration of vertebral end plates, spinal processes and likely formation of osteophytes [37]. Spinal size was observed to lead to a proximal distal shift in ^{18}F–NaF spatial uptake but less influential on ^{18}F–NaF uptake.

Using the PLSR as a patient ^{18}F–NaF uptake predictor revealed a prediction accuracy of 71 ± 3%, which was primarily due to good prediction of spatial ^{18}F–NaF uptake sites. Patient A (Fig. 7) displayed ^{18}F–NaF uptake at regions associated with small vertebral disc spacing, where the disc is highly compressed, and one site along the spinal processes. Patient B (Fig. 7) presented ^{18}F–NaF uptake concentrated around the posterior L5 to sacral region, consistent with their anterior sacral tilt. Patient C (Fig. 7) also exhibited ^{18}F–NaF uptake in the L5 vertebral body with additional concentrations on the inferior posterior L4 body. This was consistent with their moderate posterior sacral tilt and a compressed L5 – sacrum disc spacing. Our PLSR predictions of ^{18}F–NaF uptake were accurate to 71 ± 3% of the actual ^{18}F–NaF uptake. The errors were likely due to being unable to predict some of the peak magnitudes of ^{18}F–NaF. This is a likely limitation of linear PLSR and may require a nonlinear multivariate regression method, such as quadratic PLSR.

Partial Least Squares Regression (PLSR) is ideally suited to the present study as it is a multivariate linear predictor that has been reported with much success in the biology space including using femoral shape variation to rapidly reconstruct femurs [25], efficient prediction of muscle mechanics using muscle length and activation level [26], and more recently to predict a muscle volume using personalised metrics including leg length, sex and shank girth [38]. It is widely available in many open-source statistical toolkits including Scikit-learn (https://scikit-learn.org/stable/) and Tensorflow (https://www.tensorflow.org/) and works well when the variation is close to linear. Linear PLSR was reported as the best predictor of muscle volume in the recent study by Yeung et al. [38] over other machine learning techniques including support vector machine and higher order PLSR methods (that often overfit data).

There are limitations within this study that should be considered when interpreting the findings. Firstly, this study uses ^{18}F–NaF as a surrogate for lower lumbar bone degeneration and increased bone metabolic activity. Hence, patients with similar spinal shape profiles that have soft tissue related back pain are excluded. Secondly, PCA works well with populations that are consistent in shape variations, hence, people presenting with scoliosis and other pathologic bone deformities would not work as well with PCA unless they were further classified into consistent sub-categories. For this study, we removed patients who presented with scoliosis and sacralisation in order to avoid the associated limitations of PCA. Thirdly, we were limited to only 23 patients (after pathologies were removed) but it is challenging to obtain ethics to perform ^{18}F–NaF PET-CT to increase the population and we rely on historical data sets. The modelling tools presented in this study, spine population models, and ^{18}F–NaF uptake data are being made available for orthopaedic evaluation in the Musculoskeletal Atlas Project (MAP) Client (https://map-client.readthedocs.io/en/latest/), which is an open-source repository for use by the scientific and clinical communities [39] with the aim of increasing the data sets available to the scientific community. Furthermore, previous PCA has revealed that 25–30 samples is sufficient for PCA to converge [40], hence, the 23 models used for shape analysis in this study are likely close to convergence but further

investigation would be required. Fourth, patients used within this study had reached maturity, and are no longer in developmental stages, which can confound the presentation of high bone metabolism and ^{18}F–NaF uptake [41,42]. Fifth, the nature of the free-form deformation technique used in the study smooths (and filters) minor lesions and osteophytes that might explain bone degeneration and associated areas of back pain [43]. Hence, minor anatomical details may have been overlooked, but does not detract from the main shape characteristics found to correlate with ^{18}F–NaF uptake and its distribution. Finally, despite the source of ^{18}F–NaF PET-CT data coming from the same facility, different operators, historical time points, and the general low resolution of PET may contribute to noisy data. However, applied Gaussian smoothing, nearest anatomical feature mapping, and ^{18}F–NaF uptake was normalised to intensity identified in the bladder (where ^{18}F–NaF accumulates). Hence, the general study conclusions concerning ^{18}F–NaF spatial variation and anatomical correlation are less sensitive to these sources of error.

This study has revealed that the lower lumbar can be described by three main shape modes interpreted as (i) sacral tilt, (ii) vertebral disc spacing and (iii) spine size, which describe 88.7% of spine shape in our lower lumbar population. ^{18}F–NaF was described by two modes of variation including ^{18}F–NaF intensity and spatial variation (anterior-inferior to posterior-superior). ^{18}F–NaF was most sensitive to sacral tilt followed by vertebral disc spacing. Using a partial least squares regression we were able to predict ^{18}F–NaF 'hot-spot' locations with $85 \pm 5\%$ accuracy and with $71 \pm 3\%$ accuracy for the ^{18}F–NaF magnitude. These findings suggest that patients reporting with lower lumbar pain and who present with increased sacral tilt profiles and/or reduced disc spacing are good candidates for further ^{18}F–NaF PET-CT imaging, evidenced by the high association between those shape profiles and ^{18}F–NaF uptake.

This study has revealed that the lower lumbar can be described by three main shape modes interpreted as sacral tilt, vertebral disc spacing and spine size, which describe 88.7% of spine shape in our lower lumbar population. ^{18}F–NaF uptake was described by two modes of variation including ^{18}F–NaF intensity and spatial variation (anterior-inferior to posterior-superior). ^{18}F–NaF was most sensitive to sacral tilt followed by vertebral disc spacing. Using a partial least squares regression we were able to predict ^{18}F–NaF 'hot-spot' locations with $85 \pm 5\%$ accuracy and with $71 \pm 3\%$ accuracy for the ^{18}F–NaF magnitude. These findings suggest that patients reporting with lower lumbar pain and who present with increased sacral tilt profiles and/or reduced disc spacing are good candidates for further ^{18}F–NaF PET-CT imaging, evidenced by the high association between those shape profiles and ^{18}F–NaF uptake.

Declaration of competing interest

The authors have no conflicts to declare.

Acknowledgements

The authors acknowledge the support of a grant from the MedTech CoRE ART project 3709346 at the University of Auckland. The funder has played no role in the study design, in the collection, analysis and interpretation of data; in the writing of the manuscript; and in the decision to submit the manuscript for publication.

References

[1] C.E. Draper, M. Fredericson, G.E. Gold, T.F. Besier, S.L. Delp, G.S. Beaupre, A. Quon, Patients with patellofemoral pain exhibit elevated bone metabolic activity at the patellofemoral joint, J. Orthop. Res. 30 (2012) 209–213.
[2] S. Gamie, T. El-Maghraby, The role of PET/CT in evaluation of Facet and Disc abnormalities in patients with low back pain using (18)F-Fluoride, Nucl. Med. Rev. Cent. East. Eur. 11 (2008) 17–21.
[3] D.R. Fischer, Musculoskeletal imaging using fluoride PET, Semin. Nucl. Med. 43 (2013) 427–433.
[4] J.M. Cavanaugh, A.C. Ozaktay, T. Yamashita, A. Avramov, T.V. Getchell, A.I. King, Mechanisms of low back pain: a neurophysiologic and neuroanatomic study, Clin. Orthop. Relat. Res. (1997) 166–180.
[5] W.S. Marras, Occupational low back disorder causation and control, Ergonomics 43 (2000) 880–902.
[6] C.E. Dionne, K.M. Dunn, P.R. Croft, A.L. Nachemson, R. Buchbinder, B.F. Walker, M. Wyatt, J.D. Cassidy, M. Rossignol, C. Leboeuf-Yde, J. Hartvigsen, P. Leino-Arjas, U. Latza, S. Reis, M.T. Gil Del Real, F.M. Kovacs, B. Oberg, C. Cedraschi, L. M. Bouter, B.W. Koes, H.S. Picavet, M.W. van Tulder, K. Burton, N.E. Foster, G. J. Macfarlane, E. Thomas, M. Underwood, G. Waddell, P. Shekelle, E. Volinn, M. Von Korff, A consensus approach toward the standardization of back pain definitions for use in prevalence studies, Spine 33 (2008) 95–103.
[7] H.O. Svensson, G.B. Andersson, A. Hagstad, P.O. Jansson, The relationship of low-back pain to pregnancy and gynecologic factors, Spine 15 (1990) 371–375.
[8] I.H. Han, Pregnancy and spinal problems, Curr. Opin. Obstet. Gynecol. 22 (2010) 477–481.
[9] F. Tissot, K. Messing, Perimenstrual symptoms and working conditions among hospital workers in Quebec, Am. J. Ind. Med. 27 (1995) 511–522.
[10] T.P. Andriacchi, J. Favre, J.C. Erhart-Hledik, C.R. Chu, A systems view of risk factors for knee osteoarthritis reveals insights into the pathogenesis of the disease, Ann. Biomed. Eng. 43 (2015) 376–387.
[11] J. Sellam, F. Berenbaum, Is osteoarthritis a metabolic disease? Jt. Bone Spine 80 (2013) 568–573.
[12] G.M. Blake, T. Puri, M. Siddique, M.L. Frost, A.E.B. Moore, I. Fogelman, Site specific measurements of bone formation using [(18)F] sodium fluoride PET/CT, Quant. Imaging Med. Surg. 8 (2018) 47–59.
[13] G. Segall, D. Delbeke, M.G. Stabin, E. Even-Sapir, J. Fair, R. Sajdak, G.T. Smith, Snm, SNM practice guideline for sodium 18F-fluoride PET/CT bone scans 1.0, J. Nucl. Med. 51 (2010) 1813–1820.
[14] W. Langsteger, A. Rezaee, C. Pirich, M. Beheshti, 18)F-NaF-PET/CT and (99m)Tc-MDP bone scintigraphy in the detection of bone metastases in prostate cancer, Semin. Nucl. Med. 46 (2016) 491–501.
[15] M.H. Poulsen, H. Petersen, P.F. Hoilund-Carlsen, J.S. Jakobsen, O. Gerke, J. Karstoft, S.I. Steffansen, S. Walter, Spine metastases in prostate cancer: comparison of technetium-99m-MDP whole-body bone scintigraphy, [(18) F] choline positron emission tomography(PET)/computed tomography (CT) and [(18) F]NaF PET/CT, BJU Int. 114 (2014) 818–823.
[16] M. Aratake, T. Yoshifumi, A. Takahashi, R. Takeuchi, T. Inoue, T. Saito, Evaluation of lesion in a spontaneous osteonecrosis of the knee using 18F-fluoride positron emission tomography, Knee Surg. Sport. Traumatol. Arthrosc. 17 (2009) 53–59.
[17] U. Tateishi, S. Morita, T. Inoue, Diagnostic accuracy of 18F-fluoride PET and PET/CT in patients with bone metastases: a systematic review and meta-analysis update, Clin. Trans. Imag. 1 (2013) 123–134.
[18] E. Even-Sapir, E. Mishani, G. Flusser, U. Metser, 18F-Fluoride positron emission tomography and positron emission tomography/computed tomography, Semin. Nucl. Med. 37 (2007) 462–469.
[19] F.D. Grant, (1)(8)F-fluoride PET and PET/CT in children and young adults, Pet. Clin. 9 (2014) 287–297.
[20] F.W. Floeth, N. Galldiks, S. Eicker, G. Stoffels, J. Herdmann, H.J. Steiger, G. Antoch, S. Rhee, K.J. Langen, Hypermetabolism in 18F-FDG PET predicts favorable outcome following decompressive surgery in patients with degenerative cervical myelopathy, J. Nucl. Med. 54 (2013) 1577–1583.
[21] R. Bryan, P.B. Nair, M. Taylor, Use of a statistical model of the whole femur in a large scale, multi-model study of femoral neck fracture risk, J. Biomech. 42 (2009) 2171–2176.
[22] R. Bryan, P.S. Mohan, A. Hopkins, F. Galloway, M. Taylor, P.B. Nair, Statistical modelling of the whole human femur incorporating geometric and material properties, Med. Eng. Phys. 32 (2010) 57–65.
[23] C. Rao, C.K. Fitzpatrick, P.J. Rullkoetter, L.P. Maletsky, R.H. Kim, P.J. Laz, A statistical finite element model of the knee accounting for shape and alignment variability, Med. Eng. Phys. 35 (2013) 1450–1456.
[24] J. Zhang, J. Hislop-Jambrich, T.F. Besier, Predictive statistical models of baseline variations in 3-D femoral cortex morphology, Med. Eng. Phys. 38 (2016) 450–457.
[25] J. Zhang, T.F. Besier, Accuracy of femur reconstruction from sparse geometric data using a statistical shape model, Comput. Methods Biomech. Biomed. Eng. 20 (2017) 566–576.
[26] J. Fernandez, K. Mithraratne, M. Alipour, G.G. Handsfield, T.F. Besier, J. Zhang, Towards rapid prediction of personalised muscle mechanics: integration with diffusion tensor imaging, Comput. Methods Biomech. Biomed. Eng.: Imag. Vis. (2018) 1–9, https://doi.org/10.1080/21681163.2018.1519850.
[27] K.C. Assi, H. Labelle, F. Cheriet, Statistical model based 3D shape prediction of postoperative trunks for non-invasive scoliosis surgery planning, Comput. Biol. Med. 48 (2014) 85–93.
[28] F. O'Sullivan, J. O'Sullivan, A.M. Bull, A.H. McGregor, Modelling multivariate biomechanical measurements of the spine during a rowing exercise, Clin. Biomech. 18 (2003) 488–493.
[29] D. Karasik, L. Cupples, M. Hannan, D. Kiel, Genome screen for a combined bone phenotype using principal component analysis: the framingham study, Bone 34 (2004) 547–556.
[30] J. Fernandez, P. Mithraratne, S. Thrupp, M. Tawhai, P. Hunter, Anatomically based geometric modelling of the musculo-skeletal system and other organs, Biomechanics Model. Mechanobiol. 2 (2004) 139–155.
[31] J.L. Bentley, Multidimensional binary search trees used for associative searching, Commun. ACM 18 (1975) 509–517.
[32] D.Y. Tzeng, R.S. Berns, A review of principal component analysis and its applications to color technology, Color Res. Appl. 30 (2005) 84–98.

[33] S. Wold, A. Ruhe, H. Wold, W.J. Dunn, The collinearity problem in linear-regression - the partial least-squares (pls) approach to generalized inverses, SIAM J. Sci. Stat. Comput. 5 (1984) 735–743.
[34] J. Boisvert, X. Pennec, H. Labelle, F. Cheriet, N. Ayache, Principal Spine Shape Deformation Modes Using Riemannian Geometry and Articulated Models, Springer Berlin Heidelberg, Berlin, Heidelberg, 2006, pp. 346–355.
[35] T. Thireou, L.G. Strauss, A. Dimitrakopoulou-Strauss, G. Kontaxakis, S. Pavlopoulos, A. Santos, Performance evaluation of principal component analysis in dynamic FDG-PET studies of recurrent colorectal cancer, Comput. Med. Imag. Graph. 27 (2003) 43–51.
[36] P. Korovessis, M. Stamatakis, A. Baikousis, Segmental roentgenographic analysis of vertebral inclination on sagittal plane in asymptomatic versus chronic low back pain patients, J. Spinal Disord. 12 (1999) 131–137.
[37] D. Evcik, A. Yucel, Lumbar lordosis in acute and chronic low back pain patients, Rheumatol. Int. 23 (2003) 163–165.
[38] S. Yeung, J.W. Fernandez, G.G. Handsfield, C. Walker, T.F. Besier, J. Zhang, Rapid muscle volume prediction using anthropometric measurements and population-derived statistical models, Biomechanics Model. Mechanobiol. (2019) 1–11. https://doi.org/10.1007/s10237-019-01243-0.
[39] J. Zhang, H. Sorby, J. Clement, C.D.L. Thomas, P. Hunter, P. Nielsen, D. Lloyd, M. Taylor, T. Besier, The MAP Client: User-Friendly Musculoskeletal Modelling Workflows, Biomedical Simulation, Springer, 2014, pp. 182–192.
[40] J. Zhang, J. Fernandez, J. Hislop-Jambrich, T.F. Besier, Lower limb estimation from sparse landmarks using an articulated shape model, J. Biomech. 49 (2016) 3875–3881.
[41] S. Stagi, L. Cavalli, C. Iurato, S. Seminara, M.L. Brandi, M. de Martino, Bone metabolism in children and adolescents: main characteristics of the determinants of peak bone mass, Clinical cases in mineral and bone metabolism, Off. J. Italian Soc. Osteoporos. Miner. Metabo. Skelet. Muscle 10 (2013) 172–179.
[42] R.R. Recker, K.M. Davies, S.M. Hinders, R.P. Heaney, M.R. Stegman, D.B. Kimmel, Bone gain in young adult women, Jama 268 (1992) 2403–2408.
[43] T.W. O'Neill, E.V. McCloskey, J.A. Kanis, A.K. Bhalla, J. Reeve, D.M. Reid, C. Todd, A.D. Woolf, A.J. Silman, The distribution, determinants, and clinical correlates of vertebral osteophytosis: a population based survey, J. Rheumatol. 26 (1999) 842–848.